# 9

# Composite Nanomaterials for Hydrogen Technologies

Liga Grinberga and Janis Kleperis
*Institute of Solid State Physics, University of Latvia*
*Latvia*

## 1. Introduction

Analyzing today's situation and tracing tendencies, it is clear that the primary energy consumption is increasing but reserves are running out very rapidly. Meanwhile, global utilization of fossils is causing environmental problems throughout the world.

As a consequence, investigations of alternative energy strategies have recently become important, particularly for future world stability. The most important property of alternative energy sources is their environmental compatibility.

One such new energy carrier currently being investigated is hydrogen. Many hold the hopes that it could maintain mankind's growing need for energy. However, the hydrogen alternative has both positive and negative aspects.

The main advantage of hydrogen as a fuel is sustainable development. It is a non-toxic energy carrier and holds a higher energy content: 9.5 kg of hydrogen is equivalent to that of 25 kg of gasoline (Midilli, 2005). Hydrogen can be produced in many ways, however the most environmentally friendly and the less fossils consuming are processes driven directly by sunlight – photocatalysis and photo-biological methods.

Studies demonstrate that solid materials can be utilized to solve the storage problem by reversible absorption and desorption of large amounts of hydrogen (Schlapbach & Zuttel, 2001). Although several metal hydrides and composite materials are capable of meeting this target, the high desorption temperatures, slow absorption/desorption rates and small cycling capacity limit the widespread application of current metal hydrides.

Nanostructuring of materials and enhancement of surface absorption capability are two main factors to increase the amount of sorbed hydrogen. One way to combine the effectiveness of hydrogen absorption in metal hydrides and the desirable weight/volume proportion is to make composite material from alloy forming hydride and appropriate support material.

In this chapter a short description of water photocatalysis and photosynthetic hydrogen production and work of our laboratory on these subjects are given. There are described various composite materials for solid hydrogen storage and compared their characteristics. The chapter is concluded with the main results of our work on hydrogen storage in the modified $AB_5$ type metal hydride where the idea of the possible gain of using the spill-over effect to enhance catalytic activity and the amount of absorbed hydrogen was explored.

## 2. Hydrogen production

Hydrogen production is the first step toward the transition to a hydrogen economy. Fossil fuel systems for hydrogen production are the oldest technologies and tend to be the cheapest. Because fossil fuels are carbon-based, carbon dioxide is produced as a by-product when they are decomposed to release energy. Biomass pyrolysis and gasification processes are very similar to fossil fuel reforming and gasification processes.

The water splitting methods can use nuclear heat or alternative energy sources do not produce harmful emissions but they are more expensive than fossil fuel processes. Photocatalytic and photobiological processes use solar energy, and the sulphur iodine process uses nuclear heat. In the case of electrolysis, electricity supplies the energy required and there could be used alternative energy sources like wind, solar, or water power. These processes are attractive because the water feedstock contains only hydrogen and oxygen, so no carbon dioxide is released in its decomposition.

### 2.1 Photocatalysis

Photocatalytic water splitting using solar energy could be one of solutions of environmentally friendly and clean ways of hydrogen production. The basic material for the production of 'solar hydrogen' is water that is a renewable resource and on the earth it is enough and easy to access.

However, there are many problems that must be solved before this technology become economically feasible. One of tasks is the development of efficient nano sized photocatalyst that works in the visible light. The other task is to increase the efficiency of solar energy utilization.

The photochemical water splitting concept lies on the materials (photocatalysts) that can produce chemical reactions by absorption a quantum of light. The photocatalysts mainly are semiconductors that use photons to excite an electron from the valence band to the conduction band. The excited electrons by 'moving' to the conduction band and 'leaving' holes in the valence band cause reduction - oxidation reactions similarly to electrolysis (1). Electron is creating hydrogen by water molecule reduction (2) while holes form oxygen by oxidation (3) (Fig.1.).

Energy of absorbed photons must be greater than band-gap energy of a semiconductor, although the band-gap should be higher than 1.23 eV, which is the energy needed for to split water. Due to the orbital configuration of the oxide semiconductor metal cations the energy levels are more positive than oxidation potential of water and, consequently, the band-gap become wider. For ultra violet light absorption the band-gap exceeds 3 eV, however for visible light absorption the band-gap should be around 2 – 2,2 eV (Navarro et. al., 2009).

Photocatalysis reactions are considered as 'up-hill' reactions because back reactions can proceed very easy. There are several important requirements that must be fulfilled for successful photocatalytic water decomposition.

Generated electrons and holes have to be separated and before recombination reaction takes place they should migrate to the surface. In this process the bulk properties of semiconductors are determinative; tough the reduction and oxidation reactions are dependent of a surface area and active sites on the surface of a photocatalyst. Summarizing, functional photocatalyst is a complex material that should provide the right band structure and suitable bulk and surface properties.

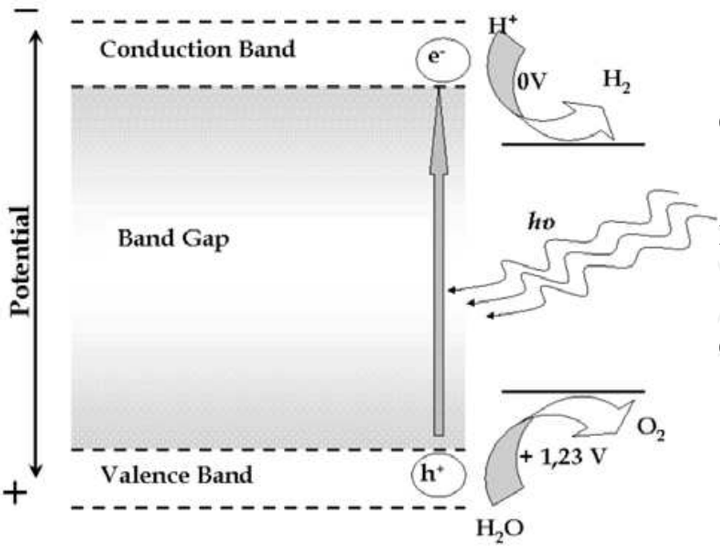


Overall reaction:

$$H_2O \rightarrow H_2 + {}^1/_2O_2 \quad (1)$$

Reduction:

$$2H^+ + 2e \rightarrow H_2 \quad (2)$$

Oxidation:

$$H_2O + 2h^+ \rightarrow 2H^+ + {}^1/_2O_2 \quad (3)$$

Fig. 1. Schematic description of water decomposition on semiconductor photocatalysts

| **Photocatalysts** | **Band-gap energy (eV)** | **Cocatalyst** | **Sacrificial reagent** | **Reference** |
|---|---|---|---|---|
| $TiO_2$-Cr-Sb | 2,2 | - | $AgNO_3$ | Kato &Kudo, 2002 |
| $SrTiO_3$ - Cr - Ta | 2,3 | Pt | $CH_3OH$ | Ishii et al., 2004 |
| $SrTiO_3$ - Cr - Sb | 2,4 | Pt | $CH_3OH$ | Kato &Kudo, 2002 |
| $La_2Ti_2O_7$ - Cr | 1,8 – 2,3 | Pt | $CH_3OH$ | Hwang et al., 2005 |
| TaON | 2,5 | Pt | $CH_3OH$ | Hitoki et al., 2002 |
| | | - | $AgNO_3$ | |
| $CaTaO_2N$ | 2,4 | Pt | $CH_3OH$ | Yamashita et al., 2004 |
| | | - | $AgNO_3$ | |
| $SrTaO_2N$ | 2,1 | Pt | $CH_3OH$ | Yamashita et al., 2004 |
| | | - | $AgNO_3$ | |
| $Sr_2Nb_2O_{7-x}N_x$ | 2,1 | Pt | $CH_3OH$ | Ji et al., 2005 |
| | | - | $AgNO_3$ | |
| $BiVO_4$ | 2,4 | - | $CH_3OH$ | Kudo et al., 1998 |
| | | - | $AgNO_3$ | |
| $(Ga_{1-x}Zn_x)(N_{1-x}O_x)$ | 2,4 – 2,8 | Cr/Rh | - | Maeda et al., 2006 |
| $(Zn_{1+x}Ge)(N_2O_x)$ | 2,7 | $RuO_2$ | - | Lee et al., 2007 |
| CdS | 2,4 | - | $S^{2-}/SO^{2-}_3$ | Navarro et al., 2008 |
| CdS - CdO - ZnO | 2,3 | - | $S^{2-}/SO^{2-}_3$ | Navarro et al., 2008 |
| $Cd_{0.7}Zn_{0.3}S$ | 2,68 | - | $S^{2-}/SO^{2-}_3$ | del Valle et al., 2008 |
| ZnS - Cu | 2,5 | - | $SO^{2-}_3$ | Kudo and Sekizawa, 1999 |
| $(AgIn)_xZn_2(1 - x)S_2$ | 2,4 | Pt | $S^{2-}/SO^{2-}_3$ | Kudo et al., 2002 |
| $(CuAg\ In)_xZn_2(1 - x)S_2$ | 2,4 | Ru | $S^{2-}$ | Tsuji et al., 2005 |
| $Na_{14}In_{17}Cu_3S_{35}$ | 2,0 | - | - | Zheng et al., 2005 |

Table 1. Selection of photocatalysts developed for water splitting reaction under visible light (Navarro et al., 2008)

To develop suitable visible light photocatalysts the band-gap tuning by doping of transition-metal cations has often been used. Unfortunately photocatalytic activity significantly decreases because doped cations inducing a formation of recombination centres between photogenerated electrons and holes and impend a migration of holes. Making a solid solution is other way of preparation of photocatalysts. There the different width band-gap semiconductor ratio can change energy levels in the composite material in total. Table 1 shows several photocatalyst materials that are developed and investigated lately.
Our group's investigations thanks to European Social Fund project 2009/0202/1DP/ 1.1.1.2.0/09/APIA/VIAA/141 lies on a developing of a new photocatalysts where the method of doping and solid solution preparation is combined.

### 2.2 Bio-hydrogen

A number of technologies for biological $H_2$ production are available, but they are not established for significant amount of hydrogen production yet. Methods for engineering and manufacturing these systems have not been fully evaluated.
Biological processes of hydrogen recovery and collection from organic resources such as municipal wastewater and sludge facilitate recycling of sewage are environmentally benign and necessary for alternative independent household support. Nowadays, many institutions and universities worldwide are involved in the research of hydrogen production by microorganisms and algae (Das & Veziroglu, 2008, Kotay Meher & Das, 2008, Donohue & Cogdell, 2006).
Microorganisms are capable of producing $H_2$ via two main pathways: fermentation and photosynthesis. The processes of bio-hydrogen production include:

1. direct biophotolysis by green algae – the photosynthetic production of hydrogen by splitting water into molecular hydrogen and oxygen using sunlight under specific conditions;
2. indirect biophotolysis by cyanobacteria with specialized cells (heterocysts) that perform nitrogen fixation and contain enzymes (nitrogenase and hydrogenase) directly involved in hydrogen metabolism and synthesis of molecular $H_2$;
3. photo-fermentation by purple non-sulfur bacteria that evolve molecular $H_2$ catalyzed by nitrogenase enzyme under nitrogen-deficient conditions using the energy of light and organic acids;
4. dark-fermentation by anaerobic bacteria grown in the dark on carbohydrate-rich substrates (Holladay et. Al., 2009, Das & Veziroglu, 2001, Levin, 2004).

Bacterial hydrogen production by fermentation of carbohydrate-containing substrates (glucose, cellulose, starch and organic waste materials) is frequently preferred to photolysis, because it does not rely on the availability of light sources. In the fermentation of glucose by enterobacteria, e.g. Escherichia coli, one of the pyruvate oxidation products, alongside with acetyl-CoA, is formate, which is produced by pyruvate formate lyase and is the sole source of hydrogen in these bacteria. The formate is split into $CO_2$ and $H_2$ by formate hydrogen lyase (FHL) complex, which comprises seven proteins, six of them being encoded hyc operon. Five hyc operon encoded proteins are membrane-embedded electron transporters. The hycE protein is one of the three E.coli NiFe hydrogenases. The hycE and FDH-H components of FHL complex are soluble peri¬plasmic proteins. The hydrogen evolved from FHL is consumed by E.coli uptake hydrogenases Hyd-1 and Hyd-2. In contrast to enterobacteria, strictly anaerobic fermenters, e.g. Clostridia, use a reduced ferredoxin

(required to oxidize pyruvate to acetyl-CoA) for $H_2$ production by the hydrogenase that generates ferredoxin in the oxidized form and releases electrons as molecular hydrogen (Nath & Das, 2004, Hallenbeck & Benemann, 2002, Maeda et. al., 2008).

Glucose fermentation by enteric bacteria yields the maximum of 2 mol H2/ mol glucose (Wang & Wan, 2009). To enhance the hydrogen production and utilize the substrate in full measure for complete conversion, the synergy of biological processes (two-stage/hybrid ones) should be applied.

Gaseous hydrogen is formed in liquid media during bacterial fermentation. Hydrogen gas hardly dissolves in aquatic solutions, but special methods are required to discharge hydrogen into atmosphere and in so doing to escape oversaturation (Mandelis & Christofides, 1993). In the atmosphere the parameters of hydrogen gas are measured by classical volumetric, mass-spectrometric and chromatography methods, or using chemical gas sensors. Wilkins (Wilkins et. al., 1974) described a method for measuring gas production by microorganisms using a platinum electrode and a reference Calomel ($Hg–Hg_2Cl_2$) electrode. To measure hydrogen gas concentration in liquid a hydrogen electrode is usually used (Pt or another noble metal − gold, rhodium, palladium, etc.).

The hydrogen H+ ions and the molecular hydrogen H2 set the equilibrium potential in compliance with the reaction: $H2 \Leftrightarrow 2H^+ + 2e^-$. This reaction proceeds very fast, so in its course the equilibrium state remains stable; in electrochemistry this electrode is adopted as zero reference (with zero potential). In microbiology, to measure dissolved oxygen and hydrogen gases the micro-respiration Clark electrodes are used (Ghirardi e.al., 1994).

In a Clark's electrode the cathode polarized versus an internal Ag/AgCl anode is placed behind an electrically insulating silicone rubber membrane, which is extremely permeable to oxygen. The flow of electrons from the anode to the oxygen-reducing cathode reflects linearly the partial oxygen pressure around the sensor tip and is in the pA range.

The same principle holds for a hydrogen Clark-type sensor: the environmental hydrogen is driven by the external partial pressure and penetrates through the sensor tip membrane to be oxidized at the platinum anode surface. Flynn et al. [Flynn et. al., 2002) used chemochromic sensors for screening in order to identify positive (i.e. hydrogen-producing) algal colonies. A chemochromic sensor film, which is normally transparent, turns blue in the presence of hydrogen gas.

Hydrogen gas is produced during the bacterial fermentation process in anaerobic conditions. In practice, hydrogen is collected in the gaseous state, since dissolved hydrogen tends to become gas. To optimize the hydrogen collection methods it is necessary to study properly the hydrogen production kinetics in liquid phase during the fermentation process. The experimental test system for bacterial hydrogen production and micro-sensors were used to determine the hydrogen gas concentrations in liquid; the mass-spectrometry method was employed for measurements in the hydrogen-containing head space.

In our experiments Escherichia coli strain MSCL 332 (i.e. from Microbial Strain Collection of Latvia) was grown on Luria-Bertani (LB) nutrient agar plates (5 g/l yeast extract, 10 g/l tryptone, 10 g/l sodium chloride, 15 g/l Bacto agar). E.coli from single colonies on the agar plates were inoculated in 2 x 150 ml flasks containing LB liquid medium. The flasks were aerobically shaken at 37°C for 12 hours at 120 rpm using a multi-shaker PSU-20.

The bacteria cell number in the overnight culture was titrated at 10-6 dilution. The amount of bacterial cell protein was calculated assuming that one E.coli cell contains $1.54 \times 10^{-13}$ g of protein. The overnight culture in LB liquid medium was mixed (1:1) with phosphate buffer

saline (PBS) pH 7.3 (0.8 g/l NaCl, 0.2 g/l KCl, 1.43 g/l $Na_2HPO_4$, 0.2 g/l $KH_2PO_4$) in a vessel sterilized for measurements. The PBS contained a complex trace element medium pH 6.5 (0.039g/l $Fe(NH_4)_2{\cdot}SO_4{\cdot}6H_2O$, 0.172 mg/l $Na_2SeO_3$, 0.02 mg/l $NiCl_2$, 0.4 mg/l $(NH_4)6Mo_7O_{24}$). Glucose (3.3mM, final concentration, sterilized through membrane 0.2µm filter) was added at the start of experiment.

The hydrogen and oxygen concentrations were measured with Clark-type microsensors in the sample liquid phase. The microsensors were connected with the signal amplifier − a pico-ammeter and an A/D current converter connected to PC using USB port.

Before the measurements, both oxygen and hydrogen microsensors were calibrated in a liquid culture medium (similar to the sample measured by 15 min bubbling Ar) for zero concentrations and hydrogen gas and clean air for 100% dissolved $H_2$ and $O_2$ concentrations (730 and 760 µmol/l, accordingly). The system is able to work independently when measurements are made in one sample. If there are several samples at a time, it is necessary to move microsensors manually and to sterilize the sensor tip using 96% ethanol, 0.1 M NaOH and distilled water every time when it is taken out from the sample.

The gas from the headspace of liquid bacterial culture in the test vessel was taken to an RGAPro-100 mass-spectrometer to analyze its components. The gas from an argon balloon through a diffuser was let in the test vessel with bacteria culture to sustain the anaerobic environment (see Fig.2) and put in a water bath to maintain a temperature of 37±2 °C.

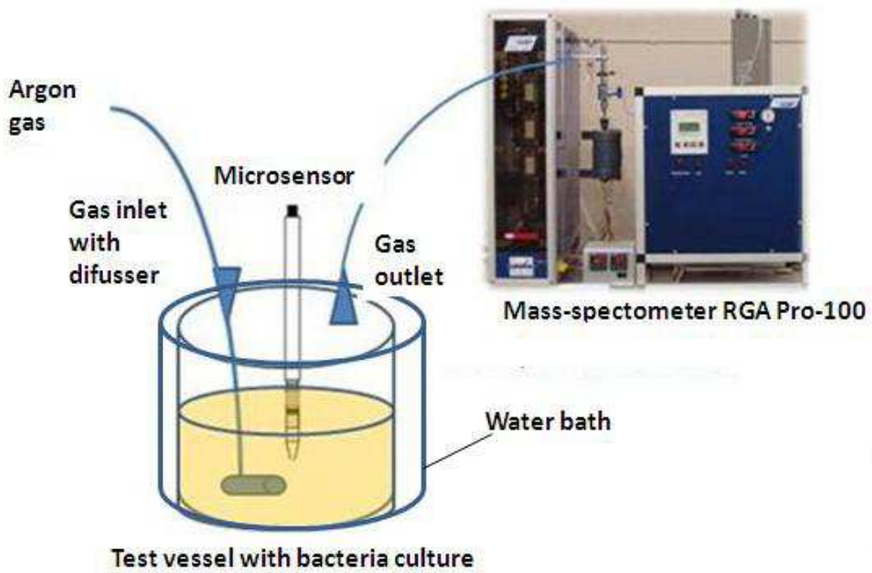


Fig. 2. Experimental test system for H2 concentration measurements with mass-spectrometer

Argon gas was bubbled through the liquid for 15 min (flow 13 l/h) and gas measurements were made with 30 min and an hour intervals. The total time of measurements was six hours. The gas volume taken for each analysis was 20 cm3. During the mass-spectrometric analysis, simultaneous measurements with a hydrogen microsensor were taken in order to make unbiased comparison of mass-spectrometric and hydrogen microsensor analyses. The concentration of dissolved hydrogen gas was measured with a microsensor; the mass-spectrometric analyses were made for the atmospheric composition in the headspace of the sample bacteria culture and nutrients.

The experimental results of microsensoric measurements were analyzed using Sensor Trace Basic and MicOX (A/S Unisense) programs, and processed by Microsoft Office Excel 2007. The mass-spectrometric data were analyzed by RGA 3.0 Software for SR Residual Gas Analyzers program.

Summarizing experiments: The hydrogen output was measured for seven hours after the beginning of fermentation process; increase in the hydrogen concentration was observed starting from the second hour after adding glucose. The constancy of oxygen concentration in the measurements evidences that the system had reliable anaerobic conditions (Fig. 3.). As is seen from this figure, the concentration of dissolved hydrogen stopped increasing after 5–10 h as glucose exhausted.

The maximum rate of hydrogen formation in the test system was 612 µmol/ l/20 min or 1.4 mmol [2.4 mg] /l per h for 43 mg protein mass (i.e. 32.6 µmol/mg protein mass). The maximum concentration of dissolved hydrogen (2481 µmol/l or 2.5 mmol/l) is reached in the fourth hour of fermentation as is seen in Fig. 2. This concentration at least three times exceeds the maximum thermodynamically allowed concentration of dissolved hydrogen in water.

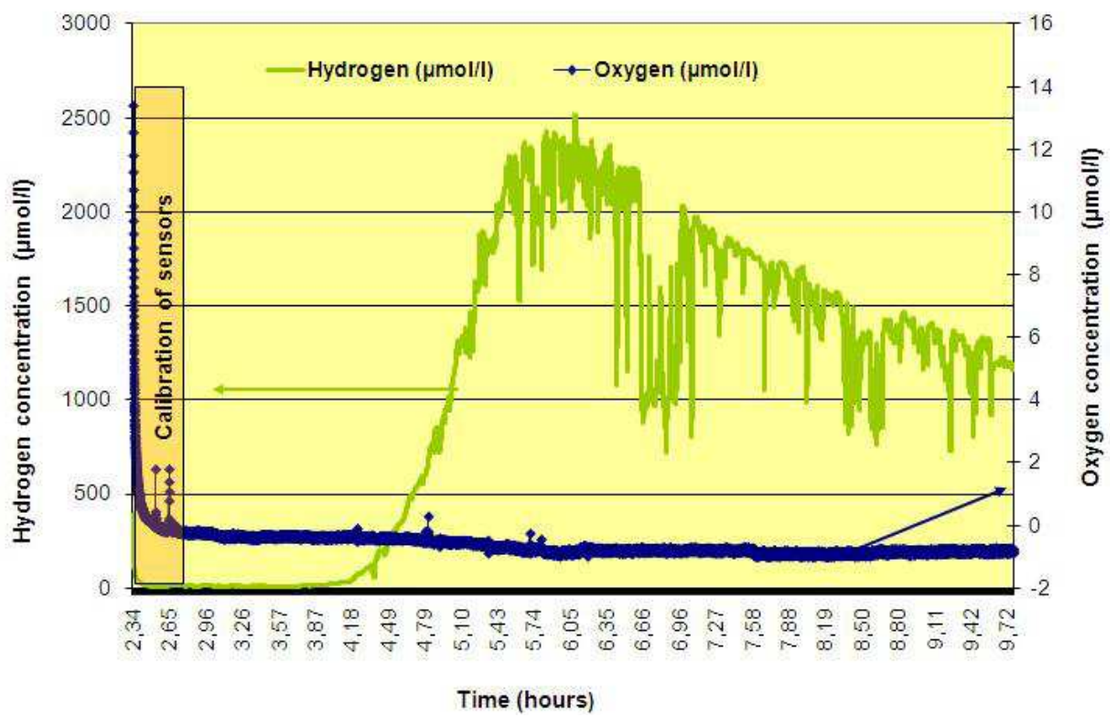


Fig. 3. Microsensoric fermentation measurements on the sample with E.coli

To demonstrate that the hydrogen production began only after glucose had been added various glucose concentrations were tested. The correlation between the glucose concentration and the hydrogen output is shown in Fig. 4.

To calculate the partial pressure of hydrogen in the headspace Henry's law was used. The calculations were done using the measured dissolved hydrogen concentrations in the test system (2481 µmol/l after 4 h fermentation). At room temperature and normal atmospheric pressure the Henry constant is $k_H$ = 1282,05 (l/atm·mol), therefore pH = 1282.05·cH (atm)

and in our case pH = 1282.05·2481·10$^{-6}$ = 3.18 atm, which obviously does not fit the experimental results obtained in the mass-spectrometric analysis.

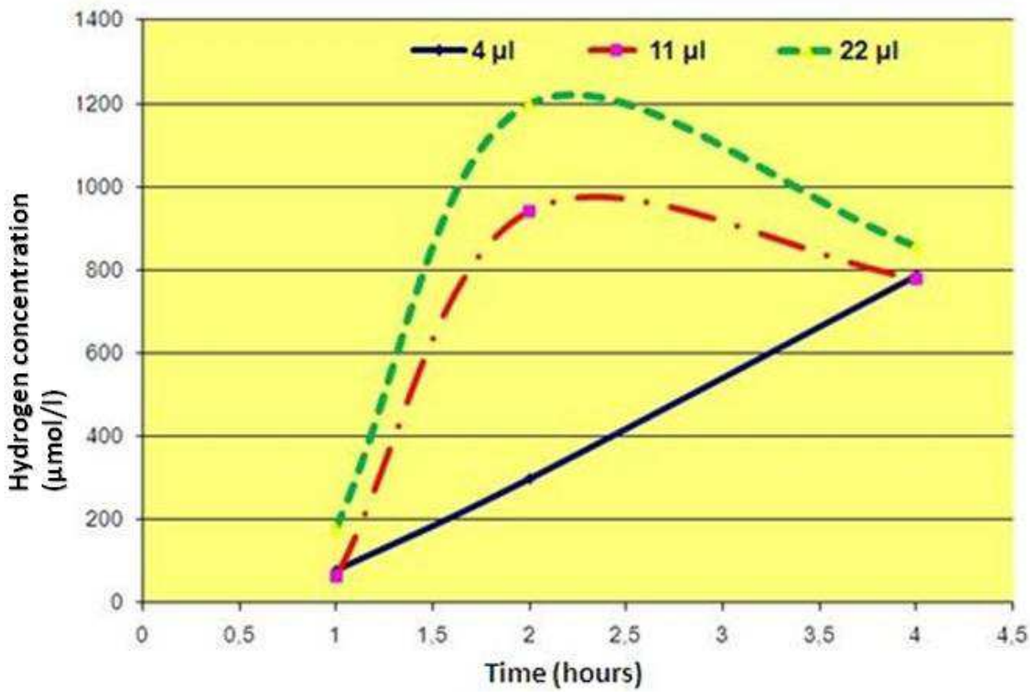


Fig. 4. Time dependence of hydrogen output at different glucose concentrations

To calculate the partial pressure of hydrogen in the headspace Henry's law was used. The calculations were done using the measured dissolved hydrogen concentrations in the test system (2481 µmol/l after 4 h fermentation). At room temperature and normal atmospheric pressure the Henry constant is $k_H$ = 1282,05 (l/atm·mol), therefore pH = 1282,05·cH (atm) and in our case pH = 1282,05·2481·10$^{-6}$ = 3.18 atm, which obviously does not fit the experimental results obtained in the mass-spectrometric analysis.

As is seen from Fig. 5, the partial pressure of hydrogen of 3.18 atm above the test system's headspace is inadequate to the concentrations determined by mass-spectrometric analysis – only 6·10$^{-3}$ atm or 0.6% vol.

The mass-spectrometric analysis has revealed the presence of different volatile substances − the end products of bacterial formation: acetate, carbon dioxide, ethanol, acteone, and hydrogen gas. In three separate measurements (without Ar bubbling and liquid mixing, with argon bubbling only, and with argon bubbling & liquid mixing) the mass-spectrometric analysis showed a hydrogen concentration increase from 0% to 0.4% after 6 h fermentation only in one measurement when no argon bubbling and mixing was applied. Such an increase in the hydrogen concentration (only 3.6·10–3 atm partial pressure) is not convincing as compared with the concentrations measured in liquid phase. A reason for that could be the limited hydrogen migration from liquid to gaseous phase (dissolved hydrogen oversaturation); besides, the mass-spectrometry measurement method was not perfect (it is to be optimized in the future experiments).

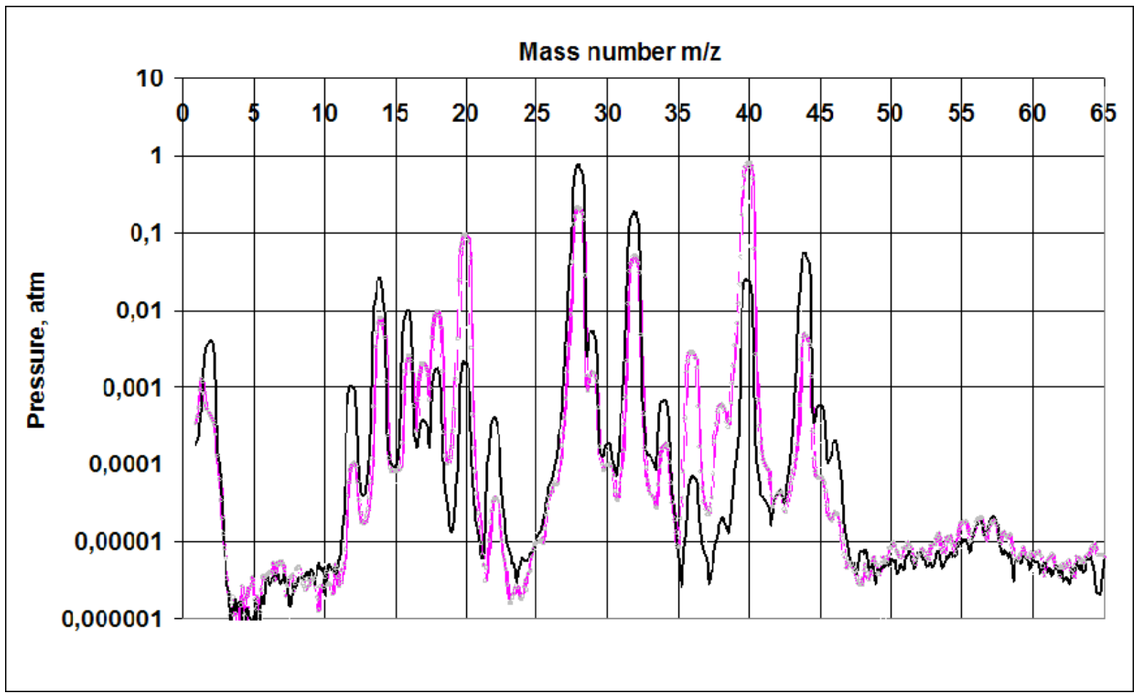


Fig. 5. Mass-spectometric analysis of the sample with bacteria E.coli before fermentation (light gray curve) and after 6h (black curve)

The mass-spectrometric analysis has revealed the presence of different volatile substances − the end products of bacterial formation: acetate, carbon dioxide, ethanol, acteone, and hydrogen gas. In three separate measurements (without Ar bubbling and liquid mixing, with argon bubbling only, and with argon bubbling & liquid mixing) the mass-spectrometric analysis showed a hydrogen concentration increase from 0% to 0.4% after 6 h fermentation only in one measurement when no argon bubbling and mixing was applied. Such an increase in the hydrogen concentration (only 3.6·10–3 atm partial pressure) is not convincing as compared with the concentrations measured in liquid phase.

A reason for that could be the limited hydrogen migration from liquid to gaseous phase (dissolved hydrogen oversaturation); besides, the mass-spectrometry measurement method was not perfect (it is to be optimized in the future experiments). Concentrations of dissolved gas are higher than theoretically possible in the anaerobic processes where gases are formed in the liquid phase and tend to reach the gas phase. Such over-saturation could be associated with biological processes: lower pH due to the formation of gases (e.g. $CO_2$, $H_2S$) in anaerobic processes; besides, a negative thermodynamic effect is caused by inhibator gases − e.g. $H_2$, since the hydrogen synthesising enzymes are sensitive to H2 concentrations and are subject to the end-product inhibition. As concentrations of hydrogen increase, its synthesis rate decreases: the evolved $H_2$ is consumed by E.coli uptake hydrogenases Hyd-1 and Hyd-2.

As mentioned, the hydrogen synthesising enzymes are sensitive to the end product − the hydrogen gas concentration. As this concentration increases the synthesis rate decreases, with formation of mixed-acid hydrogen-containing fermentation products (ethanol, acetate, butane). To enhance the hydrogen gas output, the bacterial metabolism has to be switched from alchocol and acid formation to volatile fatty acids. This can be facilitated by the

system's optimization, for example, using continuous bubbling with inert gas to reduce the partial pressure of hydrogen in the liquid phase thereby increasing its formation in the gaseous phase.
To enhance hydrogen formation, very delicate bubbling/mixing procedures should be applied, since in our measurements, with intense bubbling and mixing by a magnetic stirrer, the least hydrogen increase in the headspace was observed.

### 2.3 Conclusions

Escherichia coli wild-type strain MSCL 332 from Microbial Strain Collection of Latvia was successfully used. The hydrogen concentration in the headspace was analyzed by mass spectrometry. Due to incompleteness of the test system the hydrogen concentration in the gaseous phase was not detected, which therefore remains to be a subject of future activities. Also, the gas measuring system should be improved based on the mass-spectrometry. To enhance the transfer of dissolved hydrogen into the headspace, continuous gas bubbling and mixing are required.
The dissolved hydrogen and oxygen concentrations in liquid phase during the fermentation process were measured using microsensors. The maximum of dissolved hydrogen concentration (2481 μmol/l) was reached by the fourth hour of fermentation, which is markedly higher than predicted by Henry`s law (730 μmol/l). Also, alternative methods should be employed for the hydrogen collection directly from the nutritional broth thus making it possible to develop commercial hydrogen production.

## 3. Hydrogen storage

Hydrogen storage is clearly one of the key challenges in developing hydrogen economy and hydrogen storage for vehicle applications is one of the most important challenges.
Hydrogen storage basically implies the reduction of the huge volume of the hydrogen gas because a 1kg of hydrogen at ambient temperature and atmospheric pressure takes a volume of 11 $m^3$. To increase a hydrogen density the compressing of hydrogen or decreasing of temperature below critical must be performed.
Available technologies permit to store hydrogen directly by modifying its physical state in gaseous or liquid form in pressurized or in cryogenic tanks. Storage by absorption as chemical compounds or by adsorption on carbon materials have definite advantages from the safety perspective such that some form of conversion or energy input is required to release the hydrogen for use. A great deal of effort has been made on new hydrogen-storage systems, including metal, chemical or complex hydrides and carbon nanostructures.
Hydrogen interaction with other elements depends from material, it occurs as anion ($H^-$) or cation ($H^+$) in ionic compounds, it participates with its electron to form covalent bonds, and it can even behave like a metal and form alloys at ambient temperature. The hydrogen molecule $H_2$ can be found in various forms depending on the temperature and the pressure which are shown in the phase diagram (Fig. 5.).
The phase diagram shows that the liquid hydrogen with a density of 70.8 kg·$m^{-3}$ at -253°C only exists between the solid line and the line from the triple point at 21.2K and the critical point at 32K. At low temperature hydrogen is a solid with a density of 70.6 kg·$m^{-3}$ at -262°C and is a gas at higher temperatures with a density of 0.089886 kg·$m^{-3}$ at 0°C and a pressure of 1 bar (Zuttel, 2004).

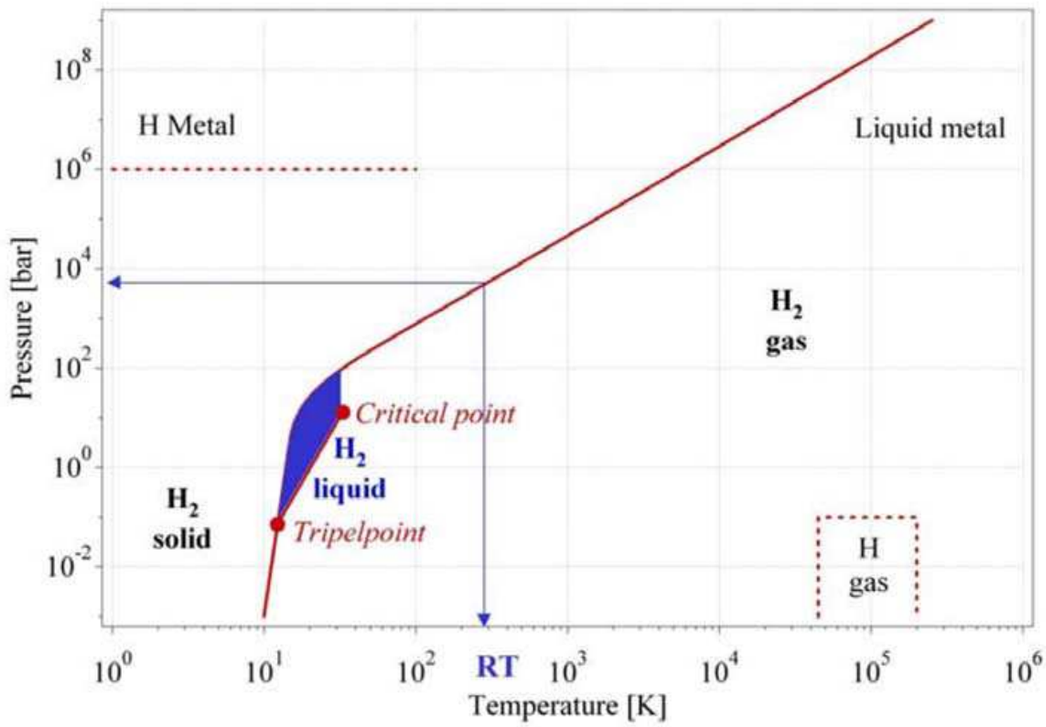


Fig. 5. Primitive phase diagram for hydrogen (Zuttel, 2004)

### 3.1 Metal hydrides

Hydrogen is a highly reactive element and forms hydrides and solid solutions with thousands of metals and alloys that will release hydrogen at elevated temperatures. Metal hydrides are arranged of metal atoms that form a host lattice, and hydrogen atoms that are installed in the interstitial sites.

The absorption process of hydrogen in the metal can be described using one-dimensional Lennard-Jones potential scheme for hydrogen molecule and 2 hydrogen atoms (Fig. 6) (Zuttel, 2004). The potential of molecule and both atoms are separated by the heat of dissociation energy $E_D$=435.99 kJ/mol in some distance from the metal surface. Approximately one hydrogen molecule radius from the metal surface the hydrogen molecule interacts with metal surface and due to the Van der Waals forces physisorption happens that is illustrated as the flat minimum in the $H_2$+M curve. Closer to the surface the hydrogen has to overcome an activation barrier for dissociation and formation of the hydrogen metal bond and hydrogen becomes chemisorbed that is showed as deep minimum of the 2H+M curve. If the both curves cross above zero energy level for the chemisorption activation energy is needed and the kinetics of adsorption is getting more slowly.

Depending on the surface elements the activation barrier height can be changed and chemisorbed hydrogen atoms may have a high surface mobility, interact with each other and form surface phases. Furthermore the chemisorbed hydrogen atom can jump in the subsurface layer and finally diffuse on the interstitial sites through the host metal lattice (Schlapbach, 1992). Hydride formation from gaseous phase can be described by pressure-composition isotherms (Fig. 7.). The host metal dissolves some hydrogen and solid solution

phase or α-phase is formed. The metal lattice expands proportionally to the hydrogen concentration by approximately 2 – 3Å$^3$ per hydrogen atom.

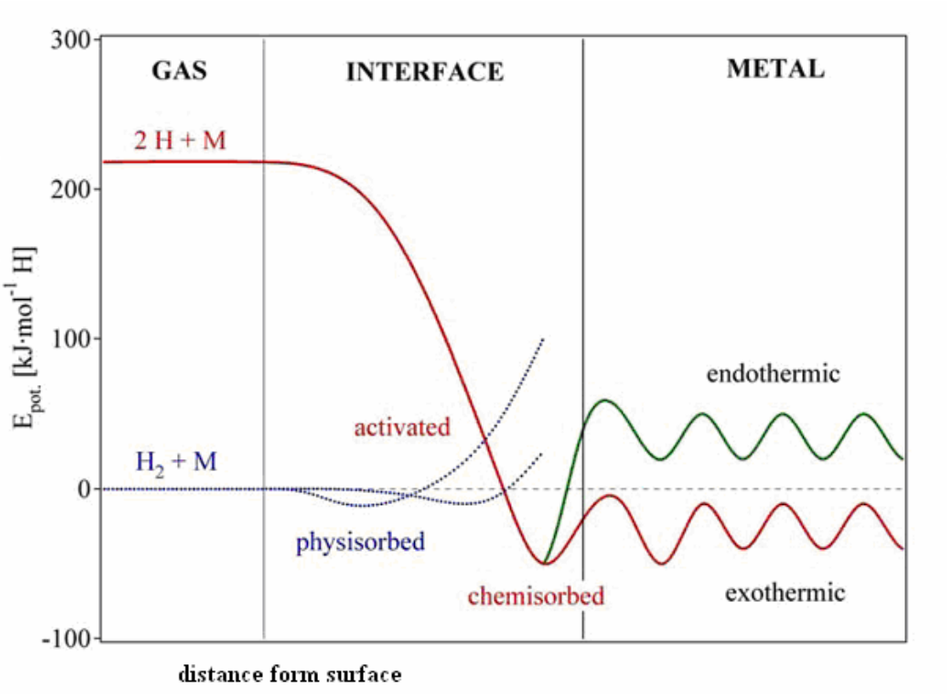


Fig. 6. Potential energy curves for activated and non-activated chemisorption of hydrogen on metal surface (Zuttel, 2003)

If the hydrogen pressure and concentration Hydrogen/Metal exceeds ratio 0,1 a H–H interaction becomes significant and the β-phase nucleates and grows. While the α-phase and β-phase coexists, the isotherms show a flat plateau, the length of which determines how much $H_2$ can be reversibly stored.

When the α-phase completely transfers to the β-phase, the $H_2$ pressure rises steeply with the concentration. Further enlargements of hydrogen pressure can cause formation of other plateaux and hydride phases. The two-phase region ends in a critical point $T_C$, above which the transition from α- to β-phase, is continuous (Fig. 7.).

The hydrogen concentration in the hydride phase is often found to be H/M=1. The volume expansion between the coexisting α- and the β-phase corresponds in many cases to 10–20% of the metal lattice. Therefore, at the phase boundary a large amount of stress is built up and often leads to a decrepitation of brittle host metals such as intermetallic compounds. The final hydride is a powder with a typical particle size of 10–100 μm (Zuttel, 2004; Schlapbach, 1998; Schlapbach, 1992).

The plateau pressure strongly depends on temperature that is related to the changes of enthalpy and entropy (4). Solving the Van't Hoff equation and from the gained slope where the pressure is a function of temperature, the heat of hydride formation can be evaluated.

$$\ln\left(\frac{p_{eq}}{p_{eq}^{0}}\right) = \frac{\Delta H}{R}\cdot\frac{1}{T}\cdot\frac{\Delta S}{R}, \tag{4}$$

where $p_{eq}$ is plateau pressure at equilibrium state, $p^0_{eq}$ stands for the plateau pressure at standard conditions, R is the universal gas constant, T is the temperature at $p_{eq}$ and $\Delta H$ is the enthalpy change.

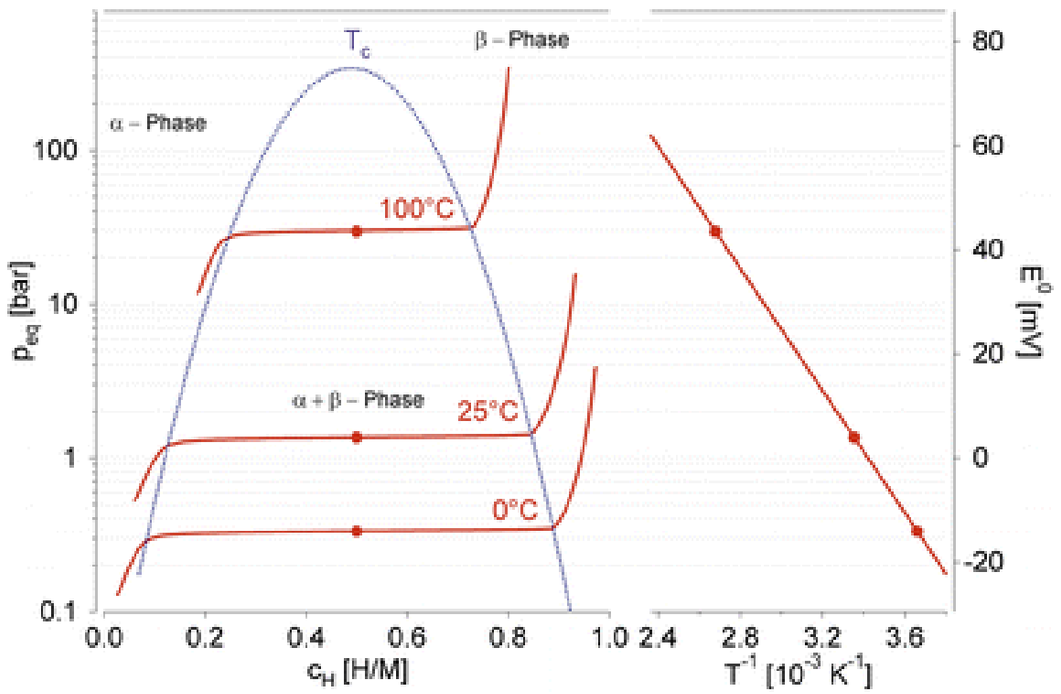


Fig. 7. Pressure composition isotherms for typical intermetallic compound is shown on the left side. The construction of the Van't Hoff plot is shown on the right hand side (Zuttel, 2004)

The enthalpy term characterizes the stability of the metal hydrogen bond. A hydride forming entropy changes leads to great heat generation during the hydrogen absorption. The same heat has to be provided to the metal hydride to desorb the hydrogen.

Hydrogen absorption is very much involved with a phase transition. Pressure does not increase with the amount of absorbed hydrogen as long as the phase transition takes place therefore a, metal hydrides can absorb large amounts of hydrogen at a constant pressure. Hydrogen sorption characteristics can be changed by partial substitution of the hydride forming elements, thereby it is possible to form some metal hydrides that works at ambient temperature and close to atmospheric pressure (Schlapbach, 1992)

A particular interest is about intermetallic hydrides because the variations of the elements allow modification of the properties of the hydrides (Table 2). The element A usually is a rare earth or an alkaline earth metal and tends to form a stable hydride or has a high affinity to hydrogen. The B element is often a transition metal and forms unstable hydrides or has a low affinity to hydrogen. The combination of the both elements A and B gives as alloys suitable for practical applications.

### 3.2 $AB_5$ intermetallic compounds

The on of the classical alloys is a combination of the La and Ni, where La individually forms $LaH_2$ at 25°C, $p=3\cdot10^{-29}$ atm, $\Delta H_f$=-208 kJ/mol $H_2$, with Ni that alone forms NiH at 25°C,

p=3400atm, $\Delta H_f$=-8,8 kJ/mol $H_2$. Although the alloy $LaNi_5$ forms a hydride at 25°C, p=1,6 atm, $\Delta H_f$=-30,8 kJ/mol $H_2$, that can be considered as a interpolation between boundaries of elemental hydride forming activities (Sandrock, 1999).

| Intermetallic compound | Prototype | Hydrides | Structure |
|---|---|---|---|
| $AB_5$ | $LaNi_5$ | $LaNi_5H_6$ | Hexagonal |
| $AB_2$ | $ZrV_2$, $ZrMn_2$, $TiMn_2$ | $ZrV_2H_{5,5}$ | Hexagonal or cubic |
| $AB_3$ | $CeNi_3$, $YFe_3$ | $CeNi_3H_4$ | Hexagonal |
| $A_2B_7$ | $Y_2Ni_7$, $Th_2Fe_7$ | $Y_2Ni_7H_3$ | Hexagonal |
| $A_6B_{23}$ | $Y_6F_{23}$, $Ho_6Fe_{23}$ | $Ho_6Fe_{23}H_{12}$ | Cubic |
| AB | TiFe, ZrNi | $TiFeH_2$ | Cubic |
| $A_2B$ | $Mg_2Ni$, $Ti_2Ni$ | $Mg_2NiH_4$ | Cubic |

Table 2. The most important hydride forming intermetallic compounds (Zuttel, 2004)

$LaNi_5$ has a $CaCu_5$-type, structure containing three octahedral and three tetragonal sites per elemental cell unit. The alloy forms at least two hydrides: α phase - $LaNi_5H_{0.3}$ - with low hydrogen content and β phase - $LaNi_5H_{5.5}$ - with high hydrogen–content. Both hydrides differ significantly in the specific lattice volume; β phase has a 25% larger lattice expansion as α phase that causes a crumbling of the alloy particles on hydriding - dehydriding cycles.

The alloy of rare earth elements in composition with nickel was used for the first time by Lindholm (Lindholm, 1996) as the electrode in the fuel cells in 1966 and then by Dilworth and Wunderlin (Dilworth & Wunderlin, 1968) in 1968. The term $MmNi_5$ was used where Mm (mischmetal)-represents a natural mixture of rare earth elements, mostly consisting of Ce (30-52 wt%), La (13 to 25 wt%), Nd, Pr and Sm (13-57 wt%) where an amount and elements of additives depends on the place of origin.

Though, the element substitutions in the $AB_5$-type alloys have been made also artificially to get better alloys for practical use. La can be replaced with Mm, Ce, Pr, Nd, Zr, Hf and Ni can be exchanged with Al, Mn, Si, Zn, Cr, Fe, Cu, Co; thereby altering the hydrogen storage capacity, the stability of the hydride phase or the corrosion resistance. For example, a partial replacement of the A and B components significantly changes macrostructure of an alloy and other properties (Table 3).

The stoichiometry of an alloy influences its durability in the long-term hydriding - dehydriding cycles, and typical commercial AB5-type alloys consists of at least 5-6 different metals, for example La0.64Ce0.36Nd0.46Ni0.95Cr0.19Mn0.41Co0.15 (Bernd, 1992).

Commonly metal hydrides are very effective for storing large amounts of hydrogen in a safe and compact way but they are mostly heavy or working in the not suitable conditions for vehicle applications. The transition hydrides are reversible and works around ambient temperature and atmospheric pressure but the gravimetric hydrogen density is limited to <3 mass%. It is still a challenge to explore the properties of the lightweight metal hydrides or investigate new hydride composite materials.

| Composition | Elements and their role |
|---|---|
| Substitutions of A in $AB_5$<br>$La_{1-y}M_yB_5$ | Zr, Ce, Pr, Nd decrease the unit cell volume, improve activation, high-rate discharge and cycle life, but increase the self-discharge due to a higher dissociation pressure of the metal hydride.<br>The use of Mm instead of La reduces the alloy costs. |
| Substitutions of B in $AB_5$<br>$A(Ni_{1-z}M_z)_5$ | A= La, Mm;M= Co, Cu, Fe, Mn, Al; $0<z<0.24$<br>**Ni** $(1-z)>2.2$ is indispensable to prevent the decrease of the amount of absorbed hydrogen and the electrode capacity<br>**Co** decreases the volume expansion upon hydriding, retards an increase of the internal cell pressure, decreases the corrosion rate and improves the cycle life of the electrode, especially at elevated temperature (40 C), but increases the alloy costs<br>**Substitution of Co by Fe** allows cost reduction without affecting cell performance, decreases decrepitation of alloy during hydriding.<br>**Al**. increases hydride formation energy, prolongs cyclic life.<br>**Mn** decreases equilibrium pressure without decreasing the amount of stored hydrogen.<br>**V** increases the lattice volume and enhances the hydrogen diffusion.<br>**Cu** increases high rate discharge performance. |
| Special additions to B in $AB_5$<br>$A(Ni,M)_{5-x}B_X$ | A= La, Mm; M = Co, Cu, Fe, Mn, Al; B= Al, Si, Sn, Ge, In, Tl,<br>**Al, Si, Sn and Ge –** minimise corrosion of the hydride electrode.<br>**Ge**-substituted alloys exhibit facilitated kinetics of hydrogen absorption/desorption in comparison with Sn-containing alloys.<br>**In, Tl, Ga** increase overvoltage of hydrogen evolution (prevent generation of gaseous hydrogen ). |
| Nonstoichiometric alloys<br>$AB_{5\pm x}$ | A= La, Mm; B=(Ni,Mn,Al,Co,V,Cu)<br>Additional **Ni** forms separate finely dispersed phase.<br>In $\mathbf{MmB_{5.12}}$ the $\mathbf{Ni_3Al}$-type second phase with high electrocatalytic activity is formed.<br>**Alloys poor in Mm** are destabilised and the attractive interaction between the dissolved hydrogen atoms increases.<br>Second phase ($\mathbf{Ce_2Ni_7}$), which forms very stable hydride is present in $MmB_{4.88}$,.<br>When $(5-x)<4.8$, the hydrogen gas evolution during overcharge decreases. |
| Addition of alloys with increased catalytic activity<br>$AB_5 + DE_3$ | D= Mo, W, Ir; E= Ni, Co<br>$DE_3$ is a catalyst for hydrogen sorption-desorptionreactions. |
| Mixture of two alloys<br>$A^1B^1{}_5 + A^2B^2{}_5$ | Mixing of two alloys characterised by various hydrogen equilibrium absorption pressures increases the electrode performance. |

Table 3. Effect on composition on properties of $AB_5$-type alloys

Our laboratory at the Institute of Solid State Physics works on the classical $AB_5$ hydride type material $LaNi_5$ modification. As hydrogen absorber, $LaNi_5$ has been one of the most investigated intermetallic compounds during the last decades. Despite of its high hydrogen capacity of a one hydrogen atom to the each metal atom and easy activation, the binary compound is not suitable for applications due to its high plateau pressure and short lifecycle (Bittner & Badcock, 1983). However, modification of the physical and chemical properties of $LaNi_5$ can be achieved by substituting lanthanum atom with a rare earth metal (e.g. Ce, Pr, Nd, Er) or nickel with a transition metal (Al, Mn, Co, Cr). Specific sample preparation methods, such as melt–spinning, sputtering and mechanical milling have been used to improve the hydrogenation kinetics of intermetallic compounds. The resulting alloys exhibit particular structural characteristics as nano-crystalline grains with a high density of grain boundaries and lack a long-range order (similar to an amorphous state). These microstructures currently provide fast hydrogenation kinetics and better lifecycle behaviour. Mechanical milling has become a popular technique because of its simplicity, relative inexpensive equipment and applicability to most intermetallic compounds. This technique has been used for several hydrogen storage alloys there was observed a good improvement in hydrogen activation and kinetics (Ares et. al., 2004, Zaluska et. al., 2001).

The diffusion of active species on the surface may play an important role in reactions on multifunctional catalyst transport phenomena. Especially, migration of hydrogen atoms from a metal to an oxide or carbon surface that by itself has no activity for dissociate hydrogen adsorption is important. It is well known that noble metals, like Pt and Pd, can adsorb and diffuse hydrogen in reactive forms over relatively large distances. This property named as spill-over effect, is widely exploited in catalysis (Scarano et. al., 2006).

The spill-over of hydrogen involves a transfer of electrons to acceptors within the support; this process modifies the chemical nature of the support and can also activate a previously inactive material and/or induce subsequent hydrogen physisorption (Roland et. al., 1997). Dissociation of hydrogen molecule on a metal and subsequent spill-over of atomic hydrogen to its support is highly dependent upon the chemical bridges formed at the interface. Hydrogen spill-over can be assessed in a number of ways, but perhaps the most common is simple calculation of the hydrogen to metal ratio, either the surface metal or total metal content. When spill-over occurs, the relation $H:M_{surface}$ will typically exceed unity. In the case of materials that form hydrides, this relation will exceed the stoichiometric ratio of the hydride.

An $AB_5$ type alloy with a trade name 7-10 produced by the company Metal Rare Earth Limited of China was chosen for experiments. To study this material the measurements were carried out using Scanning Electron Microscope (SEM) of Carl Zeiss brand, model EVO 50 XVP located at the Institute of Solid State Physics. The SEM images were taken in secondary electrons (SE); the acceleration voltage was equal to 30 kV, and the emission current was between 0,5pA and 500nA. The energy dispersive detector for X-rays (EDX) was used for composite determination in the alloy 7-10.

Structural properties of the samples were studied by X-ray Diffractometer System X-STOE Theta/theta, using Kα Cu radiation but the diffraction patterns were analyzed by appropriate software of STOE system at the DTU RISOE National Laboratory (RNL).

Tungsten – carbide crucibles with 2 balls from the same material and a high energetic ball mill Retsch® MM200 was used for grinding the raw material 7-10 for 30 minutes at frequency 25 Hz per min as well as for preparing a composite with a glass. The composite consists of 3,7 weight parts of an alloy 7-10 and of a 1 part of the Pyrex glass.

A thermogravimetric technique has been used to study the hydrogen sorption on prepared samples. The measurements were performed by equipment based on the Sartorius high pressure balance (HPB) combined with pressure, temperature and gas supplying systems. The sample is placed in the steel container that can be sealed to provide a vacuum or gas atmosphere and the pressure and temperature ranges of $10^{-3}$ - 30 bar and from room temperature to 300°C, respectively. The studied sample 340±2 mg was initially degassed under vacuum down to $10^{-3}$ bars at the ambient temperature and flushed with helium gas. That was prolonged by heating up the system until 260°C with followed vacuuming, activating at $10^{-3}$ bar hydrogen pressure and cooling down. Subsequently the previous actions were repeated two times and finished with the vacuuming of system. Afterwards, stepwise changes of the pressure inside the measuring device were applied. At a constant temperature the increase of the sample weight, as a function of time was measured for each pressure step. The same weight and treatment procedures was chosen for a composite material, though, for calculations one have to remember that in composite an amount of hydride forming alloy is less than that for pure alloy.

SEM and EDX results (Fig. 8, Table 4) shows that the composition of the alloy 7-10 corresponds to formula $A_{0,96}B_{5,04}$ (A=La, Ce, Nd, Pr; B=Ni, Co, Mn, Al, Cr) that is close to $AB_5$ stoichiometry and the molecular mass of this sample becomes 435,74 g/mol. For determination of the molecular mass of the alloy and further calculations there was assumed that after the treatment a metalhydride material contains a diminutive amount of oxygen.

The XRD pattern shows that alloy 7-10 belongs to a single phase $LaNi_5$ hexagonal $CaCu_5$-type structure in the space group P6/mmm.

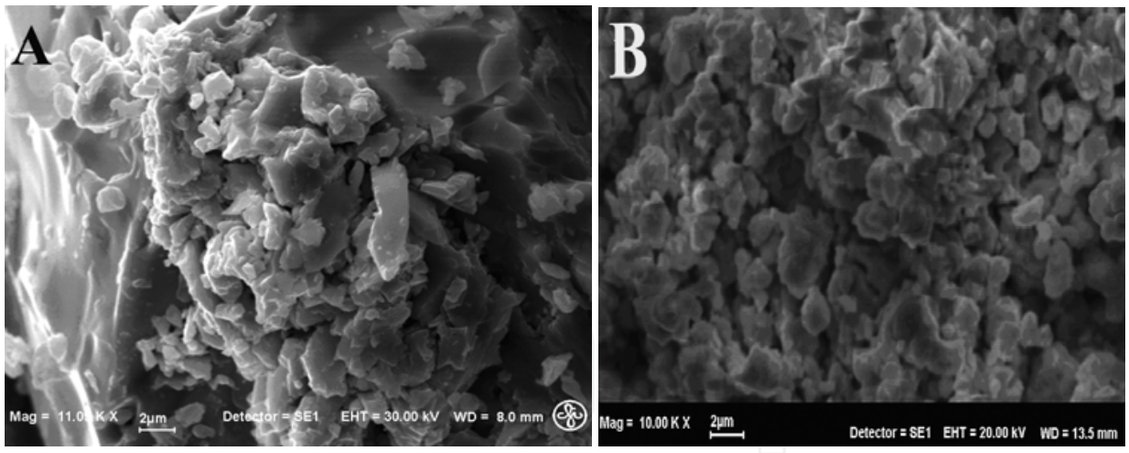


Fig. 8. SEM images of A – an alloy 7-10, grain size 50 µm and smaller, magnification 11 000; B – ball milled alloy 7-10, grain size 2 µm and smaller but agglomerated in clusters, magnification 10 000

Analysing a treated data it was figured out that a raw hydride material 7-10 absorbing more hydrogen than a classical $LaNi_5$ by itself. The HPB plots clearly shows that a pure $LaNi_5$ absorbing and desorbing hydrogen when the pressure is changed. There just a 0.26 w% of hydrogen is remaining in the pure $LaNi_5$ sample at the one atmosphere. Though, the data plot of a sample 7-10 displays opposite tendency – the absorbed hydrogen amount just slightly decreasing after lowering the pressure to the one atmosphere (Fig. 9.).

| Element | Weight % | Atomic % |
|---|---|---|
| La | 17,51 | 8,24 |
| Ce | 9,88 | 4,61 |
| Nd | 3,07 | 1,39 |
| Pr | 0,98 | 0,45 |
| Ni | 52,89 | 58,89 |
| Co | 6,23 | 6,91 |
| Mn | 5,08 | 6,05 |
| Al | 1,93 | 4,67 |
| Cr | 0,39 | 0,49 |
| O | 2,03 | 8,30 |

Table 4. Quantitative EDX data for the total surface of the sample 7-10

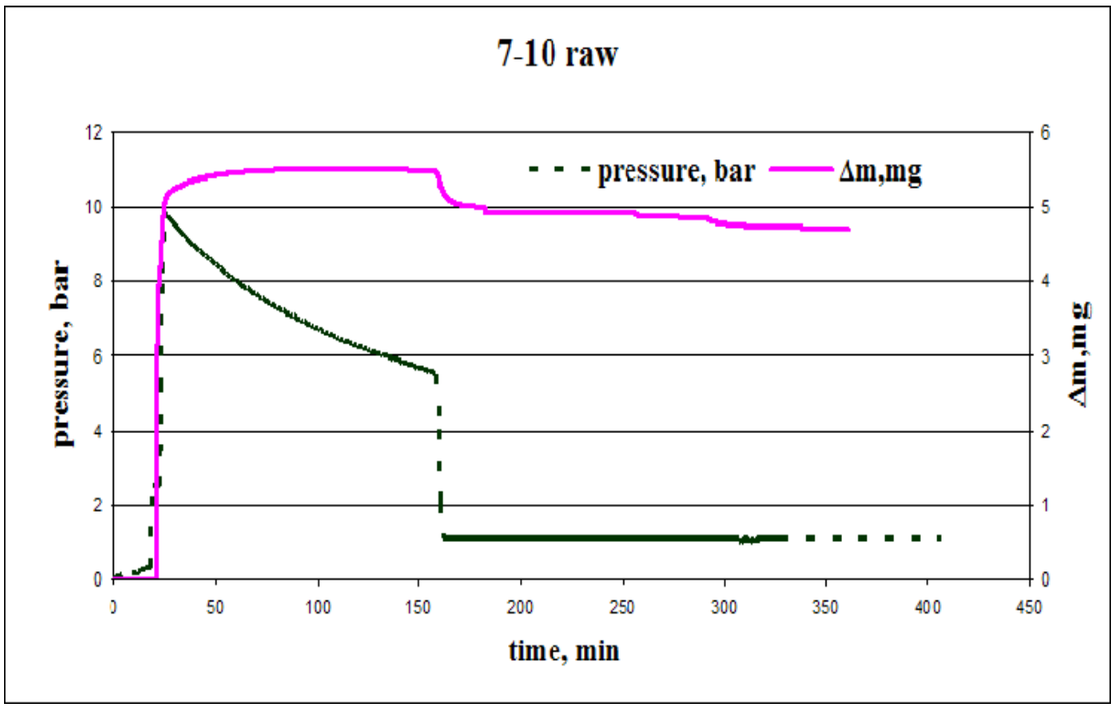


Fig. 9. HPB data plot of the raw sample 7-10 at the room temperature

Comparison of HPB results of both materials with the glass phase additives confirmed the same tendency – the composite of the alloy 7-10 and a glass absorbed more hydrogen than a composite $LaNi_5$ with a glass (Fig.10.).

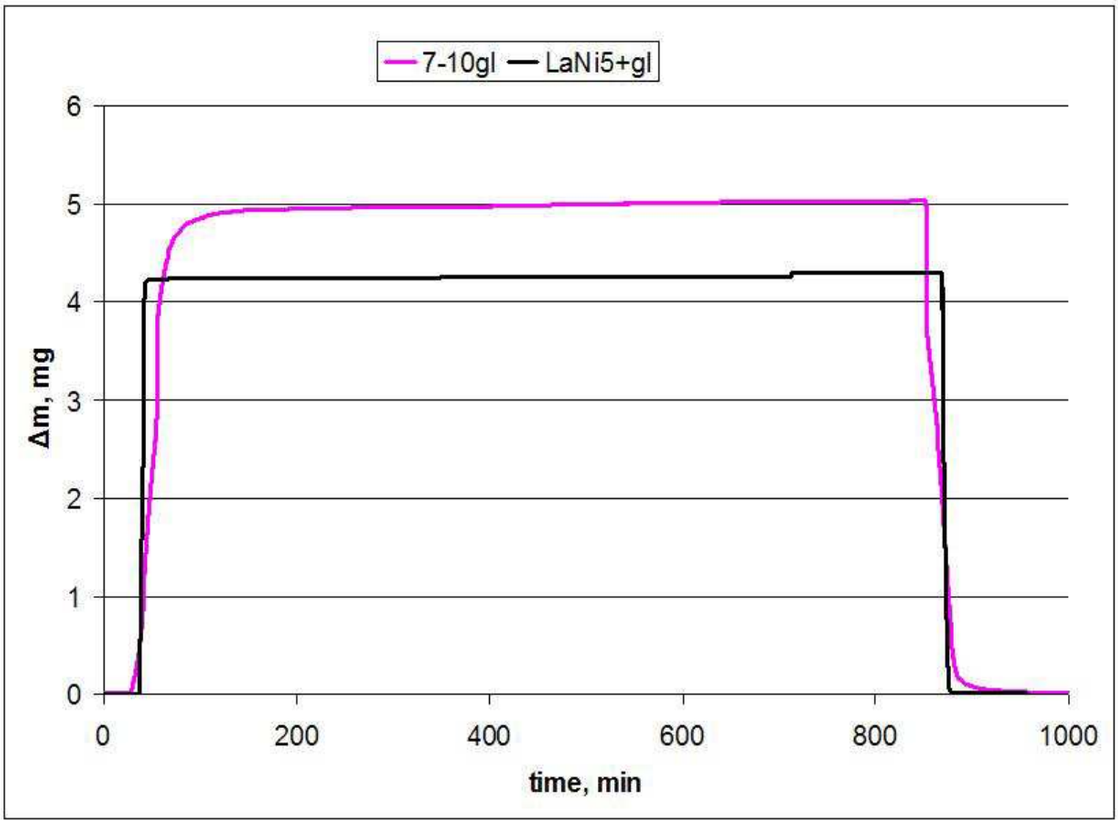


Fig. 10. HPB data of the weight change in time of the composite alloy 7-10 +glass (dashed line) and the composite $LaNi_5$ + glass (solid line)

| **7-10** | **Δm, mg** | **w%** | **x** |
|---|---|---|---|
| $\Delta m_{total}$ | 5,507E-03 | 1,582 | 6,966 |
| $\Delta m_{av}$ | 5,138E-03 | 1,477 | 6,499 |
| Δm(1atm) | 4,883E-03 | 1,405 | 6,177 |
| **7-10+glass** | **Δm, mg** | **w%** | **x** |
| $\Delta m_{total}$ | 5,048E-03 | 1,643 | 7,242 |
| $\Delta m_{av}$ | 4,616E-03 | 1,504 | 6,621 |
| Δm(1atm) | 4,393E-03 | 1,433 | 6,302 |

Table 5. Calculations of HPB data for raw alloy (7-10) and composite (7-10+glass)

The calculations of amount of the absorbed hydrogen in a raw alloy 7-10 and in the composite proved that the composite of 7-10 and glass have absorbed more than pure alloy 7-10 and are showed in the table 2, where Δm total – total change of the weight, Δmav – average change of the weight during cycling, Δm (1 atm) weight remaining at the 1 atm of

pressure, w% - weight percents of hydrogen in alloy, x = a value from stoichiometric formula of hydride $AB_5H_x$

The XRD analysis of hydrogenated samples showed a good agreement with calculations of HPB data (Fig. 11, Table 6). From the XRD plot is well observable that the diffraction peaks of the hydrogenated alloy 7-10 are largely shifted to the smaller angles than that of the starting alloy, indicating that the α-phase of hydride is changed into the β-phase and the lattice parameters and cell volume of the hydride is larger than that of the starting alloy. An observed shift of XRD peaks after hydrogenation for the composite is even larger than that for the pure 7-10 alloy. Also corresponding lattice parameters and a cell volume for the hexagonal P6/mmm symmetry accordingly is larger of hydrogenated composite sample as for fully hydrogenated alloy 7-10 (Table 6).

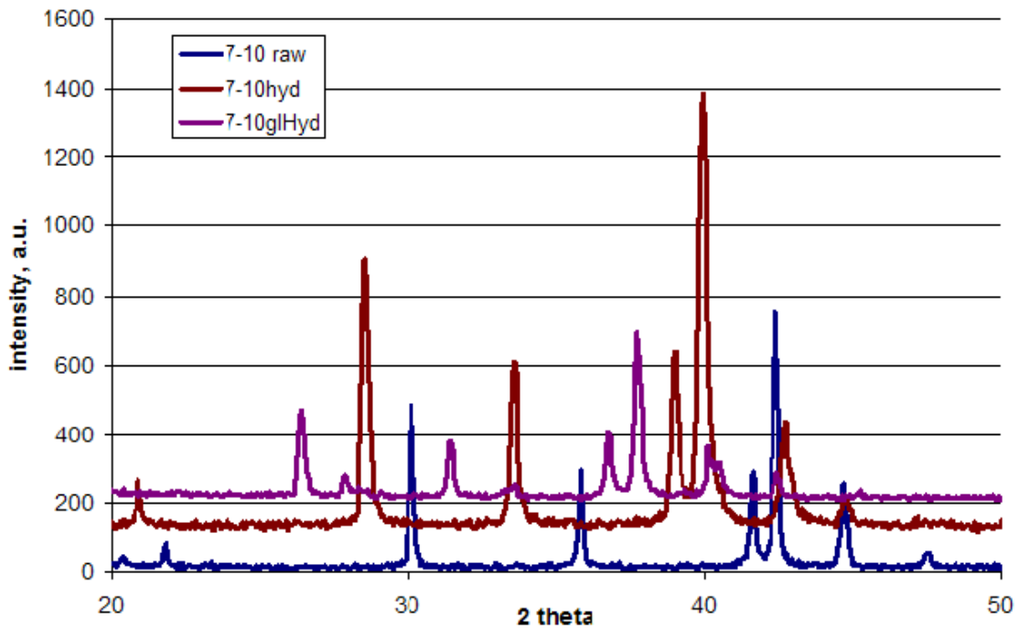


Fig. 11. XRD plot of raw (7-10raw), hydrogenated pure 7-10 (7-10H) and hydrogenated alloy 7-10 with glass phase (7-10gl-H)

| Cell size / Sample | a, Å | c, Å | V, Å3 |
|---|---|---|---|
| 7-10 | 5,0083 | 4,0567 | 88,12 |
| 7-10hydrogenated | 5,326 | 4,234 | 104,0 |
| 7-10+glass hydrogenated | 5,369 | 4,2754 | 106,78 |

Table 6. Structural parameters of raw and hydrogenated samples of alloy 7-10 and composite

### 3.3 Conclusions

The HPB data treatment and calculations showed that hydrogen uptake in the composite alloy 7-10 with glass exceeds the pure alloy that can be explained as the spillover from the

$AB_5$ catalyst. The following mechanism is deduced - the hydrogen chemisorbs at the surface sites found on the $AB_5$ (mostly Ni sites). Bridges between the catalyst and glass particles allow the chemisorbed hydrogen to migrate onto the glass surface. Desorption occurs directly from the relatively lower energy glass sites without migration back to the catalyst. Hydrogen spillover depends upon the glass-catalyst contact. The contact changes with the quality of the mixing and milling, as well as the position of alloy 7-10 grains in the mixture.
It was observed from the X-ray diffraction patterns, that the beta phase of the ball milled composite sample occurred faster than in the pure alloy sample and the peak shift to the smaller angles is noticeable larger. It is possible to assume, that the gamma hydride phase (γ) is forming when the alloy 7-10 is mixed in composite with Pyrex glass that isn't observable for pure alloy. Large lattice distortions in the γ phase are caused by hydrogen atom location sites close to Ni atoms in the elementary cell that produces inhomogeneous distribution of atoms but in the same time allows include more hydrogen atoms in the cell volume than the β phase.

## 4. References


Ares J. R., Cuevas F., Percheron-Guegan A., (2004). Influence of thermal annealing on the hydrogenation properties of mechanically milled AB5-type alloys, *Materials Science and Engineering B,*vol. 108, No. 1-2, (Apr., 2004) 76-80, ISSN 0921-5107

Bittner H. F. & Badcock C. C., (1983). Electrochemical Utilization of Metal Hydrides, *Journal of Electrochemical Society* Vol. 130, No. 5 (May, 1983) pp. 193C-198C, ISSN 0013-4651

Das.D, & Veziroglu, T.N. (2001). Hydrogen production by biological processes: a survey of literature. *Intern. J. Hydrogen Energy*, Vol. 26, No. 1, (Jan., 2001) pp. 13–28, ISSN 0360-3199

Das D., & Veziroglu N.T. (2008). Advances in biological hydrogen production processes. *Intern. J. Hydrogen Energy*, Vol. 33, No. 21, (Nov., 2008) pp. 6046-6057, ISSN 0360-3199

Dilworth L.R. & W.J. Wunderlin (1968). Allis-Chalmers manufacturing Company (US) Patent US- 3,405,008.

Donohue T.J., & Cogdell R.J. (2006). Microorganisms and clean energy. *Nature Reviews Microbiology* Vol. 4, 800. doi:10.1038/nrmicro1534 (Nov. 2006), ISSN : 1740-1526

Flynn T., Ghirardi M.L., & Seibert M. (2002). Accumulation of O2-tolerant phenoltypes in H2-producing strains of Chlamydomonas reinhardtii by sequential applications of chemical mutagenesis and selection. *Intern. J. Hydrogen Energy*, Vol. 27, No. 11-12, (Nov.-Dec., 2002) pp. 1421-1430, ISSN 0360-3199

Ghirardi M, Togasaki R.K., & Seibert M. (1997). Oxygen sensitivity of algal H2-production. *Applied Biochem Biotechnol.* Vol. 63-65, pp.141–151, ISSN: 0273-2289

Hallenbeck P.C., & Benemann J.R. (2002). Biological hydrogen production; fundamentals and limiting processes. *Intern. J. Hydrogen Energy*, Vol. 27, No. 11-12, (Nov. –Dec. 2002) pp. 1185-1193, ISSN 0360-3199

Holladay J.D., Hu J., King D.L., & Wang Y. (2009). An overview of hydrogen production technologies. *Catalysis Today*, Vol. 139, No. 4, (Jan., 2009) pp 244-260, ISSN 0920-5861

Kotay Meher S., & Das D. (2008). Biohydrogen as a renewable energy resource – prospects and potentials. Intern. J. Hydrogen Energy, Volume 33, Issue 1, January 2008, Pages 258-263 ISSN 0360-3199

Levin D.B., Pitt L., & Love M. (2004). Biohydrogen production: prospects and limitations to practical application. *Intern. J. Hydrogen Energy*, Vol. 29, No. 2, (Feb. 2004) pp. 173-185, ISSN 0360-3199

Lindholm I., (1966) Allmanna Svenska Elektriska Aktiebolaget (SE) Patent US- 3,262,816

Maeda T., Sanchez-Torres V. & Wood T.K. (2008). Enhanced hydrogen production from glucose by metabolically engineered Escherichia coli. *Applied Microbiology and Biotechnology*, Vol. 77, Nr. 4, pp. 879-890, DOI: 10.1007/s00253-007-1217-0, ISSN 1432-0614

Midilli A., Ay M., Dincer I., Rosen M. A., On hydrogen and hydrogen energy strategies: I: current status and needs., *Renewable and Sustainable Energy Reviews* Vol. 9, No. 3, (Jun., 2005) pp. 255-271, ISSN 1364-0321

Nath K., & Das D. (2004). Improvement of fermentative hydrogen production: various approaches. *Appl. Microbiol. Biotechnol.*, Vol. 65 (Oct., 2004) pp. 520–529, ISSN: 1432-0614

Navarro R.M., del Valle F., Villoria de la Mano J.A., Álvarez-Galván M.C., Fierro J.L.G. (2009) Photocatalytic Water Splitting Under Visible Light: Concept and Catalysts Development Advances in Chemical Engineering, *Advances in Chemical Engineering - Photocatalytic Technologies*, Vol.36, (Jul, 2009) pp. 111-143, ISSN: 0065-2377

Roland U., Braunschweig T., Roessner F., (1997) On the nature of spilt-over hydrogen, *Journal of Molecular Catalysis A: Chemical,* Vol. 127, No. 1-3, (Dec. 1997) pp 61-84, ISSN 0733-9372

Sandrock, G., A panoramic overview of hydrogen storage alloys from a gas reaction point of view. *Journal of Alloys and Compounds*, Vol. 293-295, (Dec., 1999) pp. 877-888, ISSN 0925-8388

Scarano D., Bordiga S., Lamberti C., Ricchiardi G., Bertarione S., Spoto D G., *Applied Catalysis A: General*,, Vol. 307, No. 1, (Jun., 2006) pp 3-12, ISSN 0926-860X

Schlapbach L., (1992) Surface properties and activation. In: *Hydrogen in intermetallic compounds II*, Vol. 67, ed. L. Schlapbach. Pp. 15-95, Springer: Berlin Heidelberg, ISBN 9780387546681, New York

Schlapbach L. and Zuttel A., (2001) Hydrogen-storage materials for mobile applications *Nature,* Vol. 414, (Nov., 2001), pp. 353-358, ISSN 0028-0836

Wang J., & Wan W. (2009). Factors influencing fermentative hydrogen production: A review. *Intern. J. Hydrogen Energy*, Vol. 34, No. 2, (Jan., 2009) pp. 799-81, ISSN 0360-3199

Wilkins J. R., Stoner G.E., & Boykin E.H. (1974). Microbial Detection Method Based on Sensing Molecular Hydrogen. *Applied Microbiology*, Vol. 5 (May 1974), pp. 949–952, ISSN 1365-2672

Zaluska A., Zaluski L., & Ström-Olsen J. O. (2001) Structure, catalysis and atomic reactions on the nano-scale: a systematic approach to metal hydrides for hydrogen storage, *Applied Physics A: Materials Science & Processing*, Vol. 72, No 2, pp. 157 – 165, ISSN 0947-8396

Züttel A., (2003) Materials for hydrogen storage, *Materials Today*, Vol. 6, No 9 (Sept., 2003) p. 24-33, ISSN 1369-7021

Züttel, A., (2004) Hydrogen storage methods. *Naturwissenschaften*, Vol. 91. No. 4, (Apr. 2004) p. 157-172, ISSN 0028-1042

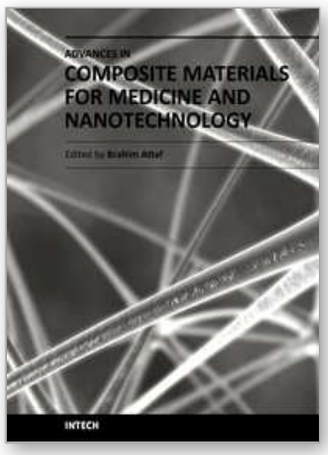


**Advances in Composite Materials for Medicine and Nanotechnology**

Edited by Dr. Brahim Attaf

ISBN 978-953-307-235-7
Hard cover, 648 pages
**Publisher** InTech
**Published online** 01, April, 2011
**Published in print edition** April, 2011

Due to their good mechanical characteristics in terms of stiffness and strength coupled with mass-saving advantage and other attractive physico-chemical properties, composite materials are successfully used in medicine and nanotechnology fields. To this end, the chapters composing the book have been divided into the following sections: medicine, dental and pharmaceutical applications; nanocomposites for energy efficiency; characterization and fabrication, all of which provide an invaluable overview of this fascinating subject area. The book presents, in addition, some studies carried out in orthopedic and stomatological applications and others aiming to design and produce new devices using the latest advances in nanotechnology. This wide variety of theoretical, numerical and experimental results can help specialists involved in these disciplines to enhance competitiveness and innovation.



**InTech Europe**
University Campus STeP Ri
Slavka Krautzeka 83/A
51000 Rijeka, Croatia
Phone: +385 (51) 770 447
Fax: +385 (51) 686 166
www.intechopen.com

**InTech China**
Unit 405, Office Block, Hotel Equatorial Shanghai
No.65, Yan An Road (West), Shanghai, 200040, China
中国上海市延安西路65号上海国际贵都大饭店办公楼405单元
Phone: +86-21-62489820
Fax: +86-21-62489821

IntechOpen